Scientific Research Publishing

Open Journal of Fluid Dynamics, 2023, 13, 122-131
https://www.scirp.org/journal/ojfd
ISSN Online: 2165-3860
ISSN Print: 2165-3852

Study of Rectangular Underexpanded Microjets

Shota Yoshimi, Shinichiro Nakao, Yoshiaki Miyazato

Department of Mechanical Systems Engineering, The University of Kitakyushu, Fukuoka, Japan
Email: d2mba027@eng.kitakyu-u.ac.jp

How to cite this paper: Yoshimi, S., Nakao, S. and Miyazato, Y. (2023) Study of Rectangular Underexpanded Microjets. *Open Journal of Fluid Dynamics*, **13**, 122-131.
https://doi.org/10.4236/ojfd.2023.132010

Received: April 12, 2023
Accepted: May 27, 2023
Published: May 30, 2023

Abstract

The underexpanded microjet emerging from a rectangular convergent nozzle with a high aspect ratio at the nozzle exit is investigated numerically using the Reynolds-averaged Navier-Stokes (RANS) simulation with the Menter's shear stress transport (SST) k-ω turbulence model. The simulation is performed at the nozzle pressure ratio of 5.0 to produce a strong shock and it is validated by a comparison with a rainbow schlieren picture of the microjet. The three-dimensional structure of the shock-containing rectangular microjet is demonstrated using the isopycnic surface and bright-field schlieren representations.

Keywords

Microjets, Rainbow Schlieren, RANS Simulation, Rectangular Nozzle, Shock Waves

1. Introduction

Microjets issuing from rectangular nozzles with high aspect ratios (AR: the ratio of the major dimension to the minor dimension at the nozzle exit) have been widely used because of their practical applications in mechanical devices such as air knives in manufacturing, gas wiping in continuous steel strip galvanizing line [1], and so on. However, little is known about the flow characteristics of such planar microjets because of challenging issues.

Kashimura *et al.* [2] carried out the Reynolds-averaged Navier-Stokes (RANS) simulation with the compressible k-ω turbulence model of a jet issuing from a two-dimensional convergent nozzle with a height of 1 mm at the exit. The nozzle pressure ratio (NPR) defined as the ratio p_{os}/p_b of the plenum pressure p_{os} to the back pressure p_b was varied over a range of NPRs from 1.893 to 6.0 to investigate the structures and shock cell spacings of two-dimensional underexpanded microjets. Handa *et al.* [3] applied the molecular tagging velocimetry (MTV) for

supersonic microjets issuing from a convergent-divergent nozzle with a design Mach number of 2.0 and a rectangular shape of 500 μm × 5000 μm (AR = 10) at the exit. They clarified effects of the Reynolds number on the microjet structure including the supersonic core length and the velocity decay process. Aniskin *et al.* [4] [5] measured the Pitot pressures along the central axis of free jets issuing from flat convergent micronozzles with height from 175 μm to 22.3 μm and the corresponding aspect ratio from 22 to 116 at the exit and acquired the shock-cell spacing as well as the supersonic core length. Subsequently, Aniskin *et al.* [6] investigated effects of the Pitot microtube diameter on the main parameters of plane underexpanded microjets such as the shock-cell spacing and the supersonic core length. Two convergent nozzles with sizes of 22.3 μm × 2593 μm (AR = 116) and 83.3 μm × 3823 μm (AR = 46) at the nozzle exit and two glass Pitot tubes with inner diameter (μm)/outer diameter (μm) of 24/70 and 16/42 were used in the experiments. As a result, they found that the length of the first shock-cell measured by the Pitot microtube is overestimated in comparison with that visualized by the shadowgraph method, but the Pitot tube diameter has a minor effect on the supersonic core length.

In the present study, the flow structure of a shock-containing microjet emerging from a rectangular convergent nozzle with a high-aspect ratio of 10 at the exit is visualized using the rainbow schlieren deflectometry. In addition, the flow field of rectangular microjet is simulated by solving the RANS equations to clarify the near-field shock structure quantitatively. The Menter's shear-stress transport (SST) k-ω turbulence model is used for the simulations because it has been widely used and trusted model in areas of aerospace community [7]. Three-dimensional flow structure of the rectangular shock-containing microjet is displayed by computer flow visualizations.

2. Experimental Method

The experiments were conducted in a blowdown compressed-air facility in the High-Speed Gasdynamics Laboratory at the University of Kitakyushu. Since the facility has been described in detail elsewhere [8] [9] [10], only a brief description is given in the present paper. Ambient air is pressurized by the compressor up to 1 MPa and stored in a high-pressure reservoir comprising two storage tanks with a total capacity of 2 m^3 after filtering and drying. The high-pressure dry air from the reservoir gets stagnated in the plenum chamber; subsequently, it is discharged into the atmosphere through a test nozzle that can be rotated about its central axis. The desired NPR (p_{os}/p_b) is achieved by changing the plenum pressure, p_{os}, with the back pressure, p_b (=atmospheric pressure), held constant at 5.0 to produce strong shocks in the jet plume.

As shown in **Figure 1**, a rectangular convergent nozzle with an aspect ratio of 10 at the nozzle exit was used as the test nozzle. The Cartesian coordinate system (x, y, z) is employed with its origin at the center of the nozzle exit plane; the x-, y-, and z-axes are oriented along the directions of the nozzle major axis, minor

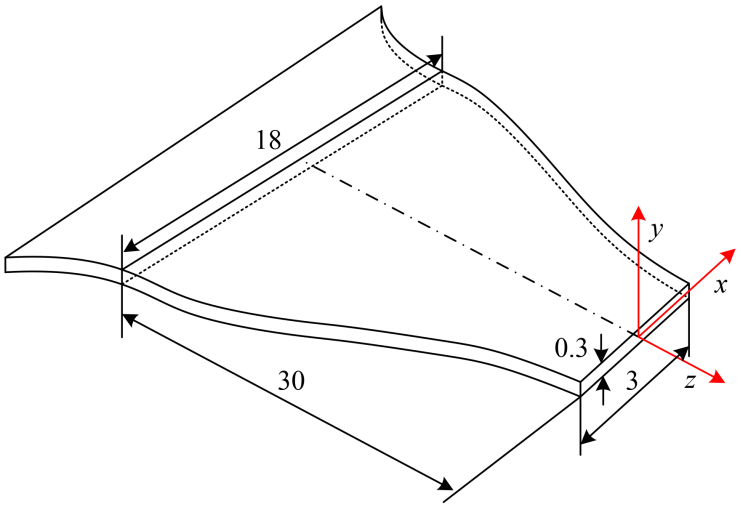

Figure 1. Schematic diagram of test nozzle. All dimensions are in mm.

axis, and central axis, respectively. The major and minor dimensions of the nozzle inlet are 18 mm and 300 μm, respectively, and the corresponding ones at the nozzle exit are $w = 3$ mm (spanwise width) and $h = 300$ μm (vertical height), respectively. The axial length from the nozzle inlet to the exit is 30 mm. The nozzle has a constant height of 300 μm between the upper and lower walls over the whole distance from the nozzle inlet to exit, while it is designed by a sinusoidal curve for the nozzle side walls between the nozzle inlet and exit to provide smooth uniform and parallel flows at the exit.

The jet flow fields were visualized through rail-mounted optical components, including a spatial filter with a rectangular source aperture of 3 mm × 50 μm; two achromatic lenses with a diameter and focal length of 25 mm and 250 mm, respectively; a rainbow filter with a continuous hue variation at a width of 2.4 mm; and a digital camera (Nikon D7100, 6000 × 4000 square pixel resolution with a 14-bit pixel depth) fitted with a focusing lens with a diameter and focal length of 30 mm and 600 mm, respectively. A continuous 250 W metal halide light source (Sigmakoki, IMH-250) connected to a fiber optic cable with a diameter of 50 μm provides light input to the spatial filter through an objective lens with a focal length of 16.56 mm. The rainbow filter was introduced into the focal plane (schlieren cutoff plane) of the decollimating lens vertically with respect to the nozzle axis. This filter setting corresponds to the vertical knife edge in the conventional schlieren system.

The camera outputs of rainbow schlieren images in the RGB format were transferred onto a personal computer hard drive using the Nikon Camera Control Pro software and then stored as JPEG files. Each JPEG RGB image (8-bit each) was turned into an HSI image (8-bit each) according to the hue (H)-saturation (S)-intensity (I) representation obtained from direct transformation of the RGB tristimulus values. The hue (H) values transformed only were utilized to calculate the ray shift at the cutoff plane of the schlieren system. This means that a unique hue can be transmitted to the image plane from a given location on the

filter plane. Thus, the ray shift on the filter plane could be related to the hue measured in the image plane.

3. Numerical Method

The structures of shock-containing microjets issuing from a rectangular convergent nozzle with an aspect ratio of 10 at the exit are investigated numerically using the commercial CFD software ANSYS Fluent Version 16.0. The geometry of the test nozzle used in the RSD experiments is modeled by subtracting the solid sections of the nozzle from the control volume. The center on the nozzle exit plane is taken as the origin, *i.e.*, $x = y = z = 0$, where x and y denote the major and minor axis directions, respectively, and z shows the axial direction. The pressure-based compressible RANS equations are numerically solved. The Menter's SST k-ω turbulence model is employed because Sugawara *et al.* [11] [12] showed that the RANS simulations with this turbulence model for round shock-containing microjets are in good quantitative agreement with experimental density fields captured by the Mach-Zehnder interferometry. The NPR is held constant at 5.0 where p_{os} and p_b are 500 kPa and 100 kPa, respectively, and the plenum temperature T_{os} upstream of the nozzle is specified at 300 K. The dry air is assumed to follow the perfect gas law with a constant specific heat ratio of $\gamma = 1.4$, and the coefficient of viscosity is calculated by using the Sutherland's formula.

The solid walls including the nozzle wall are treated as adiabatic and no-slip, and all the boundaries except for the left boundary are the pressure outlets (*i.e.*, p_b is specified). The structured mesh is generated by the mapped face meshing function equipped with ANSYS Fluent, and the total mesh count is approximately 41 million elements with 41 million node points. The grid spacing within a region of -1.5 mm $\le x \le 1.5$ mm, -150 μm $\le y \le 150$ μm and 0 mm $\le z \le 10$ mm is relatively uniform and fine (10 μm) in order to resolve the complex shock cell structures. Inside the nozzle, the grid size smoothly decreases in the direction perpendicular with respect to the wall surface to capture the boundary layer. The size of the lowest grids near the nozzle wall surface is around 10 μm, which corresponds to 0.8 in terms of the non-dimensional variable y^+. To accurately capture the fine structures of shock-containing jets, we set a minimum mesh interval to 10 μm in the vicinity of the nozzle exit.

After performing a grid sensitivity analysis, we confirm that the RANS calculation with this grid resolution can predict the flow flowfield with a reasonable agreement with the experimental data. The CFL number is set based on the pseudo transient under-relaxation method. The UPWIND-type finite volume schemes with the van Albada limiter are used to achieve the second-order accuracy in space. The spatial gradients of the flow variables are calculated in a pre-processing step at all vertices using a Green-Gauss approach and then averaged to obtain these gradients at the cell faces when computing viscous fluxes along the edges. For the time-integration, the three-stage Runge-Kutta method is used. We iterate the solution sufficiently enough so that the residuals of all equa-

tions reduce by an order of three, indicating that solution seem to converge.

4. Results and Discussion

4.1. Density Gradient Fields

Figure 2 shows comparisons of experimental rainbow schlieren pictures (upper half) and numerical density gradient fields (lower half) for rectangular underexpanded microjets. They indicate the flow structures at the minor and major axis plane views, respectively. Note that the simulation results denote the streamwise density gradient fields on the cross-section including the jet central axis. On the other hand, the rainbow schlieren pictures display the streamwise density gradient

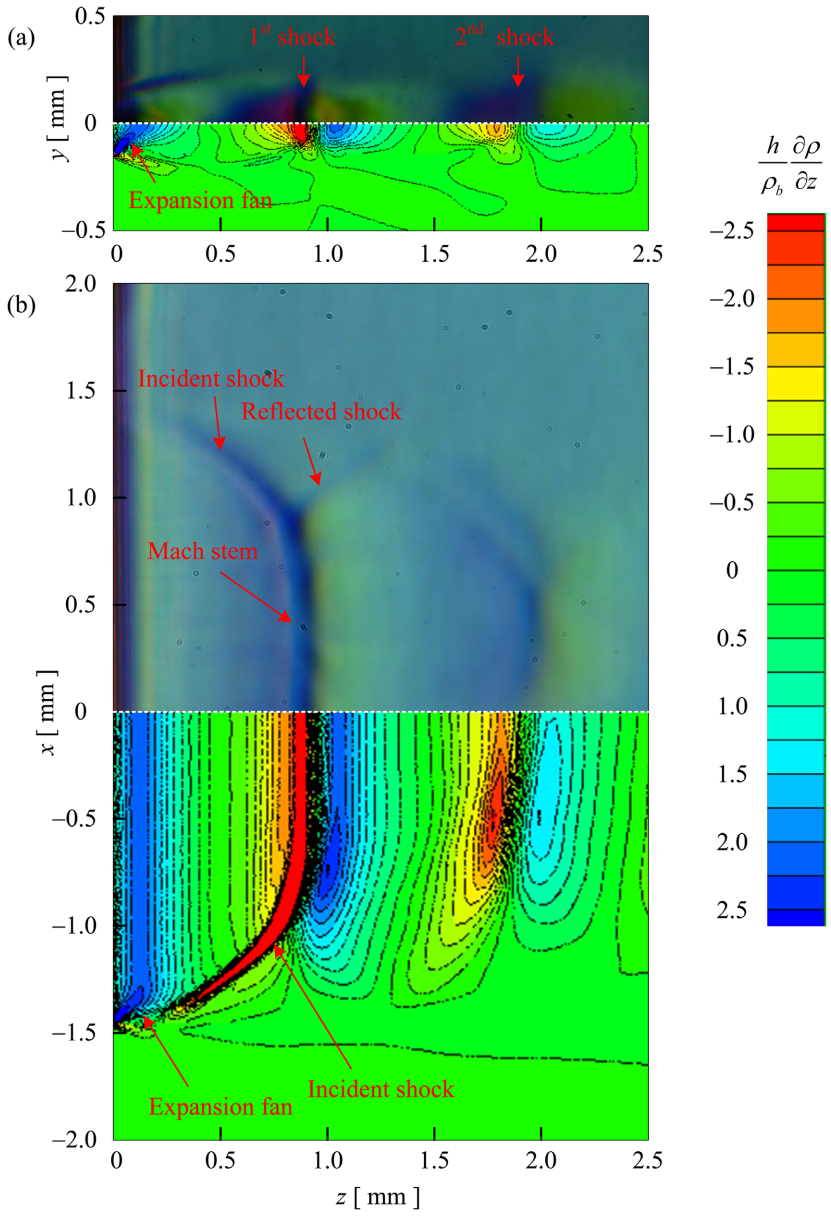

Figure 2. Rainbow schlieren pictures and density gradient fields in the (a) minor axis plane and (b) major axis plane of a rectangular underexpanded free jet.

that is integrated along the light-of-sight direction.

Figure 2(a) shows that the jet in the minor plane view exhibits an archetypic shock-cell structure of rectangular shock-containing jets where two shocks can be seen in both figures. In addition, one can see convex shocks. The numerical result also reproduces the jet structure in the corresponding schlieren picture quite well. The rainbow schlieren picture in Figure 2(b) demonstrates that the jet of the major axis plane view includes a Mach shock composed of a long Mach stem, a short incident shock, and a short reflected shock in the first shock-cell due to the relatively high pressure ratio (NPR = 5.0). The simulated shock shapes in the major axis plane are in good agreement with the experimental ones except that the short reflected shock is observed in the experiment. The difference between experiment and simulation can be probably attributed to the difference between the density gradient averaged in the viewing direction and the density gradient in the cross-section including the central axis of the jet.

4.2. Three-Dimensional Density Fields

The three dimensional flow feature of the rectangular shock-containing microjet can be demonstrated with an isopycnic surface as shown in Figure 3 where the density field is normalized by the ambient density ρ_b. Although the expansion and compression regions within the first shock-cell between the nozzle exit ($z = 0$ mm) and z = around 0.5 mm show two dimensional structure except for the jet outer boundaries, the following downstream shock-cells exhibit three-dimensional flow features. The length in the x-direction for the expansion region shown in blue inside each shock cell is smaller downstream. We plan to reproduce such a

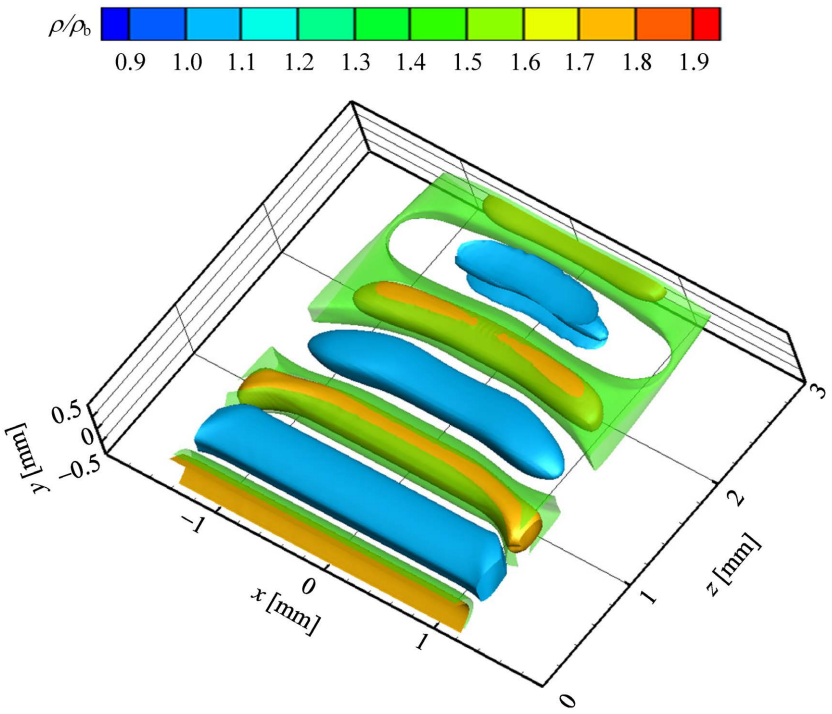

Figure 3. Isopycnic surface of a rectangular underexpanded free jet.

three-dimensional density field using the rainbow schlieren tomography and Mach-Zehnder tomography.

The density fields in the cross section including the central axis of the jet are shown in Figure 4(a) and Figure 4(b) for the minor axis plane and major axis plane, respectively. The density fields are normalized by the ρ_b. The levels of the contour are presented at the right of the figure as a color bar. The size of the expansion and compression regions inside the shock-cells gradually decreases in the flow direction in the minor axis plane and major axis plane. The density in the x direction in the major axis plane is not constant for a fixed z. The location of the maximum density inside the first shock-cell is not immediately after the

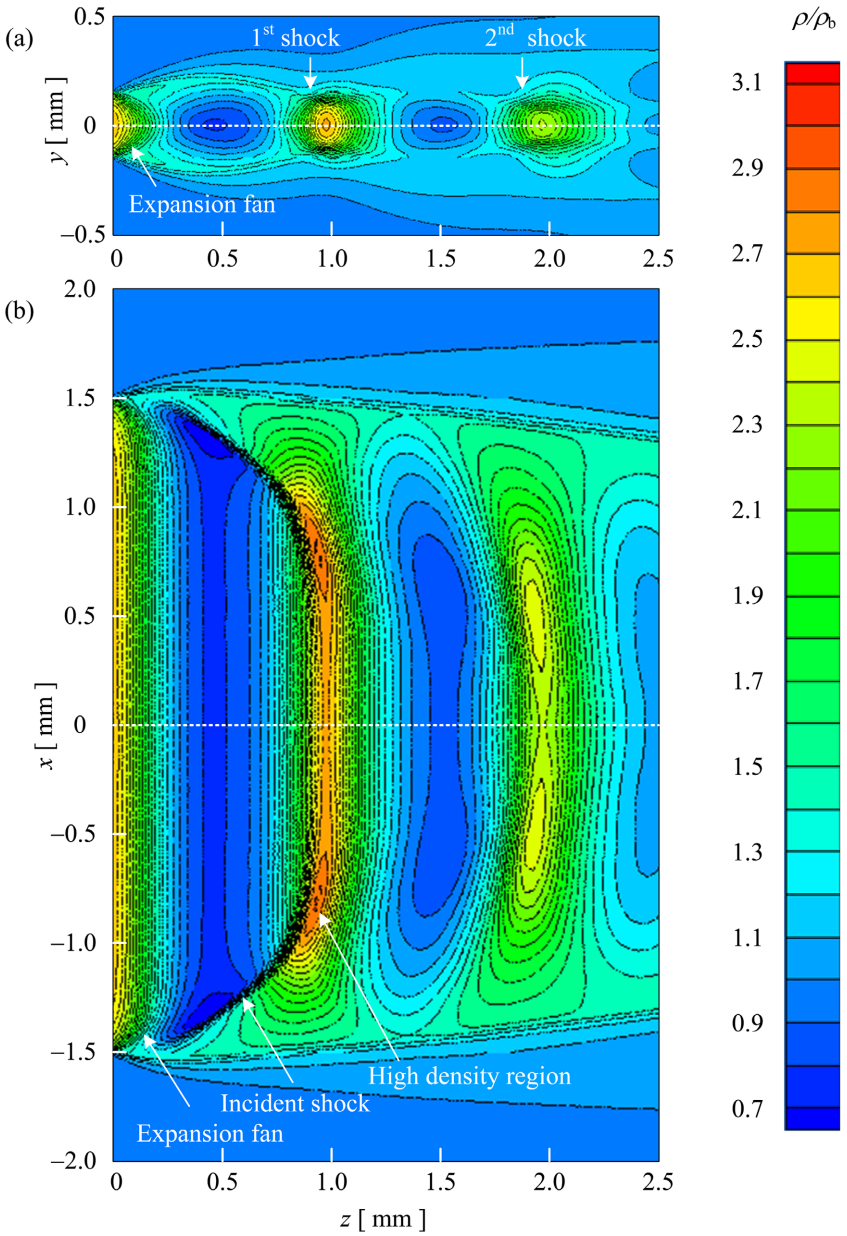

Figure 4. Density fields in the (a) minor axis plane and (b) major axis plane of a rectangular underexpanded free jet.

incident shock on the central axis of the jet, but just downstream of the two points where the incident shock bends.

4.3. Shock Dynamics

Shock dynamics can be expressed using the magnitude of the density gradient vector [13], which can be represented by highlighting regions where the density gradient is spatially steep such as the root of expansion waves and shocks. The projections of the magnitude of the density gradient vector onto the *zy* and *zx* planes are shown in **Figure 5(a)** and **Figure 5(b)**, respectively. These are sometimes called the bright field schlieren [12] [14] or the circular-cutoff schlieren,

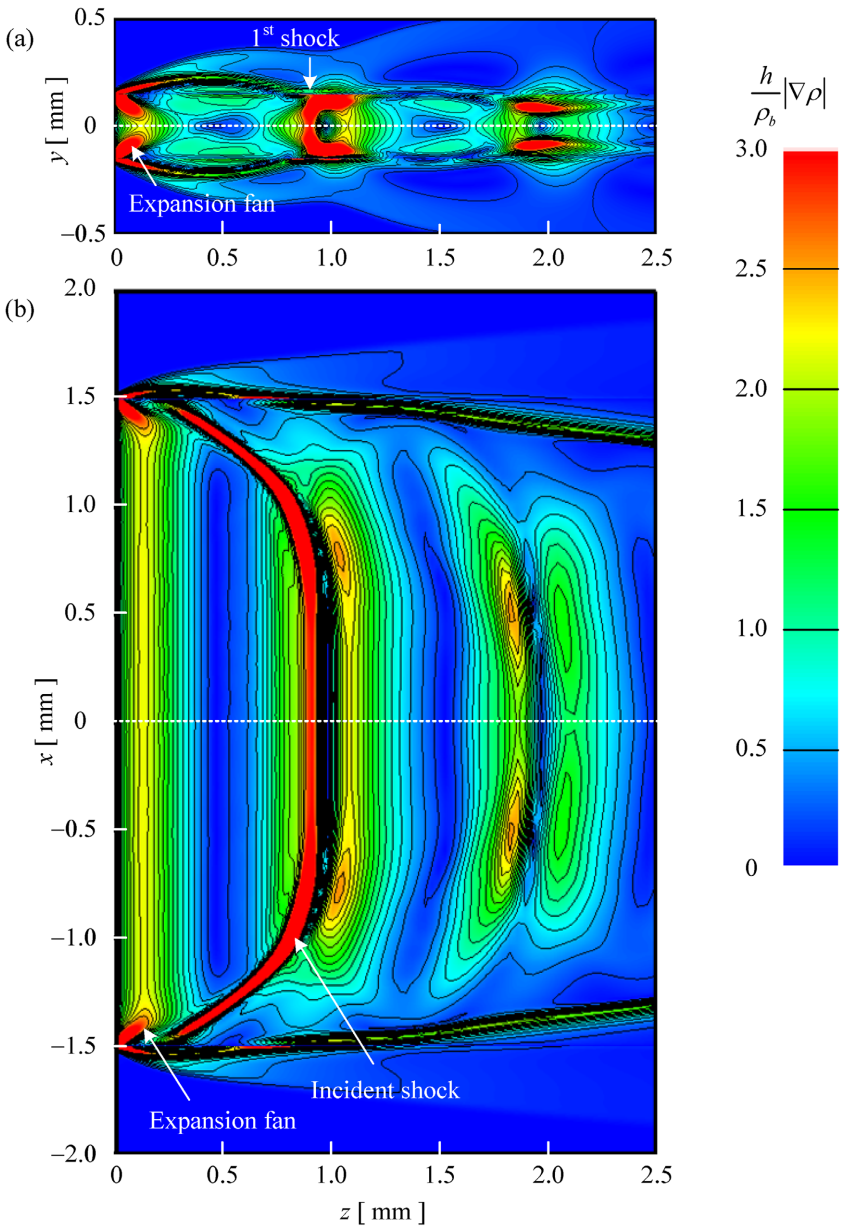

Figure 5. Bright field schlierens in the (a) minor axis plane and (b) major axis plane of a rectangular underexpanded free jet.

which corresponds to schlieren with a disc-shaped filter.

Figure 5 demonstrates that the two-dimensional shape of the shock as well as jet boundary and the regions where the expansion waves are generated can be clearly observed. The spatial evolution of the jet near-field shock structure can be clearly seen three-dimensionally. It can be seen that the incident shock originates immediately after the expansion waves from the nozzle exit lip. The shock inside the second shock-cell in the major axis plane is stronger away from the central axis rather than on the central axis. Since the shock inside the second shock-cell is weaker than the incident shock, its shape can hardly be observed.

5. Conclusion

A shock-containing microjet emerging from a rectangular convergent nozzle with a high aspect ratio of 10 at the exit was examined numerically using the RANS simulations with the Menter's SST k-ω turbulence model where the nozzle has a rectangular area of a 3 mm wide and a 300 μm high at the exit. The nozzle pressure ratio was held constant at 5.0 to produce a strong shock in the jet plume. Comparisons of the simulated density gradient fields in the flow direction in the minor axis and major axis planes of the jet with the rainbow schlieren pictures showed relatively good agreement. The jet three-dimensional structure was demonstrated numerically with the isopycnic surface. The shock dynamics in the near-field region was expressed using the bright field schlieren. In the future, it is desirable to obtain reliable experimental values that can directly validate numerical calculations. In addition, it is necessary to investigate the effects of other numerical codes on the microjet structure.

Acknowledgements

This work was supported in part by Grant-in-Aid for Scientific Research (C) (Grants No. 20K04272 and No. 20K04290).

Conflicts of Interest

The authors declare no conflicts of interest regarding the publication of this paper.

References

[1] Kweon, Y.H. and Kim, H.D. (2011) Study on the Wiping Gas Jet in Continuous Galvanizing Line. *Journal of Thermal Science*, **20**, 242-247. https://doi.org/10.1007/s11630-011-0465-6

[2] Kashimura, H., Masuda, Y., Miyazato, Y. and Matsuo, K. (2011) Numerical Analysis of Turbulent Sonic Jets from Two-Dimensional Convergent Nozzles. *Journal of Thermal Science*, **20**, 133-138. https://doi.org/10.1007/s11630-011-0447-8

[3] Handa, T., Mii, K., Sakurai, T., Imamura, K., Mizuta, S. and Ando, Y. (2014) Study on Supersonic Rectangular Microjets Using Molecular Tagging Velocimetry. *Experiments in Fluids*, **55**, 1725. https://doi.org/10.1007/s00348-014-1725-5

[4] Aniskin, V.M., Maslov, A.A., Tsirulnikov, I.S. and Timofeev, I.V. (2015) Visualiza-

tion of Supersonic Axisymmetric and Plane Underexpanded Microjets. *Journal of Flow Visualization & Image Processing*, **22**, 213-227. https://doi.org/10.1615/JFlowVisImageProc.2016016429

[5] Aniskin, V.M., Maslov, A.A., Mironov, S.G., Tsyryulnikov, I.S. and Timofeev, I.V. (2015) An Experimental Study of the Structure of Supersonic Flat Underexpanded Microjets. *Technical Physics Letters*, **41**, 508-510. https://doi.org/10.1134/S106378501505017X

[6] Aniskin, V.M., Timofeev, I.V., Maslov, N.A. and Tsibulskaya, E.O. (2019) Effect of the Pitot Microtube Diameter on Pressure Measurement in Plane Supersonic Microjets. *Flow Measurement and Instrumentation*, **70**, 101655. https://doi.org/10.1016/j.flowmeasinst.2019.101655

[7] Franquet, E., Perrier, V., Gibout, S. and Bruel, P. (2015) Free Underexpanded Jets in a Quiescent Medium: A Review. *Progress in Aerospace Sciences*, **77**, 25-53. https://doi.org/10.1016/j.paerosci.2015.06.006

[8] Fukunaga, R., Ezoe, M., Nakao, S. and Miyazato, Y. (2022) Application of Rainbow Schlieren Tomography for Shock-Containing Rectangular Jets. *Journal of Visualization*, **25**, 687-695. https://doi.org/10.1007/s12650-022-00827-w

[9] Nagata, T., Islam, M.M., Miyaguni, T., Nakao, S. and Miyazato, Y. (2022) Shock-Cell Spacings of Underexpanded Sonic Jets Emerging from Elliptic Nozzles. *Experiments in Fluids*, **63**, 111. https://doi.org/10.1007/s00348-022-03463-0

[10] Tashiro, T., Fukunaga, R., Utsunomiya, D., Nakao, S., Miyazato, Y. and Ishino, Y. (2023) Flow Features of Underexpanded Microjets Emerging from a Round Convergent Nozzle. *Experiments in Fluids*, **64**, 55. https://doi.org/10.1007/s00348-023-03603-0

[11] Sugawara, S., Nakao, S., Miyazato, Y., Ishino, Y. and Miki, K. (2020) Three-Dimensional Reconstruction of a Microjet with a Mach Disk by Mach-Zehnder Interferometers. *Journal of Fluid Mechanics*, **893**, A25. https://doi.org/10.1017/jfm.2020.217

[12] Sugawara, S., Nakao, S., Miyazato, Y., Ishino, Y. and Miki, K. (2020) Quantitative Flow Visualization of Slightly Underexpanded Microjets by Mach-Zehnder Interferometers. *Flow, Turbulence and Combustion*, **106**, 971-992. https://doi.org/10.1007/s10494-020-00211-4

[13] Maeno, K., Kaneta, T., Morioka, T. and Honma, H. (2005) Pseudo-Schlieren CT Measurement of Three-Dimensional Flow Phenomena on Shock Waves and Vortices Discharged from Open Ends. *Shock Waves*, **14**, 239-249. https://doi.org/10.1007/s00193-005-0256-7

[14] Settles, G.S. and Hargather, M.J. (2017) A Review of Recent Developments in Schlieren and Shadowgraph Techniques. *Measurement Science and Technology*, **28**, 042001. https://doi.org/10.1088/1361-6501/aa5748